Preparation of Controllable Crystalline Titania and Study on the Photocatalytic Properties

Maocheng Yan,[†] Feng Chen,[†] Jinlong Zhang,*[,†] and Masakazu Anpo[‡]

Lab for Advanced Materials and Institute of Fine Chemicals, East China University of Science and Technology, 130 Meilong Road, Shanghai 200237, P.R. China, and Department of Applied Chemistry, Graduate School of Engineering, Osaka Prefecture University, 1-1 Gakuen-cho, Sakai Osaka 599-8531, Japan

Received: August 30, 2004; In Final Form: March 3, 2005

Nanocrystalline TiO_2 catalysts with different anatase/rutile ratios and high surface area (113−169 m^2/g) have been prepared at low temperature by the microemulsion-mediated hydrothermal method. The samples were characterized by x-ray diffraction (XRD), Fourier transform (FT)-IR spectra, UV−vis diffuse reflectance spectra, and nitrogen adsorption−desorption methods. The contents of anatase and rutile phases in the TiO_2 powders have been successfully controlled by simply changing the proportion of Cl^- and SO_4^{2-} in the aqueous phase of the microemulsion. A proposed mechanism involving bidentately chelated sulfate is discussed to explain the variation of the crystalline phase in the TiO_2 powder. The photodegradation of methyl orange (MO) in water has been investigated over titanium dioxide consisting of different anatase/rutile ratios. The catalyst containing 74.2% anatase showed the highest photocatalytic activity, which is due to a synergistic effect between anatase and rutile. The synergism was also found for the photodegradation of MO with physically mixed anatase and rutile as catalysts.

1. Introduction

Since the discovery of photoelectrochemical splitting of water on *n*-TiO_2 electrodes,[1] titania-mediated heterogeneous photocatalysis has attracted extensive interest because of its potential applications to environment protection. Between the two main kinds of crystalline TiO_2, anatase has been confirmed to have quite high photocatalytic activity in the photodegradation of most pollutants in water[2] and in air,[3−5] while the photocatalytic activity of rutile is still indistinct. Most work has shown that rutile is a very poor photocatalyst,[6] while some has reported that rutile could have a higher activity than anatase when it has small crystalline size;[7] Sclanfani et al.[8] observed that the rutile phase is active or inactive according to the preparation conditions to some extent. However, it is widely accepted that the mixed phase of titania is beneficial in reducing the recombination of photogenerated electrons and holes, and it always results in an enhancement of photocatalytic activity.[9−12] Degussa P-25, which naturally consists of about 80% anatase and 20% rutile with a Brunauer−Emmett−Teller (BET) surface area of 50 m^2/g, was extensively studied as a standard titania catalyst partially because of its high photocatalytic activity which profits from the mixed phase of anatase and rutile.[13−16] Thus, it is very important to develop a synthetic method in which the crystalline phase of titania can be controlled.

Inorganic additives, such as Al_2O_3[17] and ZrO_2,[18] have been successfully utilized to control the anatase/rutile phase transformation in the TiO_2 preparation. However, it is difficult to clear the inorganic additives off of the final products and/or avoid the possible influence of additives to photocatalytic activity. Recently, some controllable synthesis processes of crystalline nano-TiO_2 have been developed without any inorganic additives. Luo et al.[19] synthesized bicrystalline (anatase and rutile) and tricrystalline (anatase, rutile, and brookite) mesostructured titania by varying the solvent and cosolvent. Liu and co-workers[20] prepared rutile/anatase mixtures by controlling the content of toluene-*p*-sulfonic acid in a homogeneous hydrolysis system and subsequent heat treatment. However, both of their synthetic methods need a heat treatment at high temperature in order to get crystalline titania and result in the increase of crystalline size and the decrease of the surface area. Wu et al.[21] successfully synthesized rutile and anatase with the microemulsion-mediated hydrothermal (MMH) method at low temperature. In Wu's microemusion method, hydrochloric acid or nitric acid was used as the hydrolysis inhibitor of tetrabutyl titanate. When the concentration of hydrochloric acid in the microemulsion was more than 1.0 M, the product was pure rutile phase. However, when the concentration of nitric acid was 0.5 M, the product was mainly attributed to anatase phase. Although this work did not show us a precise manner of controlling the crystalline phase of TiO_2, it exhibited a possibility of stepwise adjustment of the percentage of anatase and/or rutile phase in the titania product. Therefore, in our work, hydrochloric acid and sulfate were selected as two adjustors in the process of TiO_2 preparation. By simply varying the proportion of anion in the aqueous phase of microemulsion, controllable crystalline nano-TiO_2 with high surface area was successfully synthesized at low temperature. To confirm the effect of the crystalline phase distribution on the photocatalytic activity of prepared TiO_2, the photocatalytic activity of TiO_2 with different percentages of anatase and/or rutile was tested for the photodegradation of methyl orange.

2. Experimental Section

2.1. Preparation of the Catalysts. For the preparation of the reverse microemulsion system, Triton X-100 (*tert*-octylphenoxypolyethoxyethanol) was used as the surfactant, *n*-hexanol as the cosurfactant, and cyclohexane as the continuous oil phase. Tetrabutyl titanate and $(NH_4)_2SO_4$ were dissolved in the

* Corresponding author. Fax: +86-21-64252062. E-mail: jlzhang@ecust.edu.cn.
[†] East China University of Science and Technology.
[‡] Osaka Prefecture University.

10.1021/jp046087i CCC: $30.25
Published on Web 04/05/2005

hydrochloric acid as the aqueous phase. The synthetic procedure was as follows: First, 10 mL of Triton X-100, 6 mL of *n*-hexanol, and 16 mL of cyclohexane were mixed under magnetic stirring. Second, 3.4 mL of tetrabutyl titanate and 0.0682 g of $(NH_4)_2SO_4$ were dissolved in 4 mL of 10 M hydrochloric acid solution, making up the aqueous phase. Then, the aqueous phase was added dropwise to the oil phase, forming the clear microemulsion. All of the above steps were carried out at room temperature. The microemulsion was transferred into a 100-mL Teflon-inner-liner stainless-steel autoclave. The autoclave was kept for 13 h below 120 °C, and then, precipitate was collected at the bottom of the autoclave. The precipitate was washed repeatedly with ethanol and water to remove the oil, surfactant, cosurfactant, and acid, and then dried for 12 h in an infrared oven to obtain the final sample S-1.28, in which the number "1.28" refers to the mole percentage of SO_4^{2-} in the Cl^- and SO_4^{2-} ($n_{SO_4^{2-}}/(n_{Cl^-} + n_{SO_4^{2-}}) \times 100$). Different samples of S-1.60, S-1.12, S-0.96, S-0.80, S-0.64, and S-0.32 were also prepared by the same procedure, except the mole percentage of SO_4^{2-} was adjusted to the corresponding value. The samples of S-100 and S-0.00 were prepared by the same method in which the aqueous phase was formed by dissolving 3.4 mL of tetrabutyl titanate into 4 mL of 10 M hydrochloric acid and 4 mL of 5 M sulfuric acid solution, respectively. No further heat treatment was done for all samples.

2.2. Catalyst Characterization. XRD measurements were carried out with a Rigaku D/max 2550 VB/PC apparatus at room temperature using Cu Kα radiation and a graphite monochromator, operated at 40 kV and 100 mA. UV−vis diffuse reflectance spectra (DRS) were obtained for the dry-pressed disk samples using a Scan UV−vis−NIR spectrophotometer (Varian Cary 500) equipped with an integrating sphere assembly, using $BaSO_4$ as the reflectance sample. The BET specific surface areas (S_{BET}) of the samples were determined by the N_2 adsorption−desorption method at 77 K (Micromeritics ASAP 2010). All the samples were degassed at 393 K before measurement. FT-IR spectroscopy was performed on a Nicolet Magna 550 spectrometer with KBr beam-splitter. Spectra were collected with a resolution of 4 cm^{-1} by using 100 scans.

2.3. Photocatalytic Experiments. The MO was used as a simulated contaminant in this work. Degradation experiments were carried out by adding 0.06 g of TiO_2 powder into an 80-mL quartz photoreactor containing 60 mL of a 40 mg L^{-1} MO solution. The concentration of the catalyst was 1 g L^{-1}. The mixture was sonicated for 10 min and stirred for 30 min in the dark in order to reach the adsorption−desorption equilibrium for MO and dissolved oxygen before illumination. The stirred suspensions were illuminated with a 300-W high-pressure Hg lamp for which the strongest emission wavelength is 365 nm. The average light intensity striking the TiO_2 powder was about 1230 $\mu W/cm^2$, as measured by a UV radiometer (made in the Photoelectric Instrument Factory of Beijing Normal University) with the peak intensity of 365 nm. The lamp was cooled with flowing water in a quartz cylindrical jacket around the lamp, and ambient temperature is maintained during the photocatalytic reaction because of good ventilation. The pH of the solution is 4.75 and not adjusted further (The pH of deionized water is about 5.73). The group of MO molecules adsorbed on the TiO_2 surface is mainly the sulfonic acid group under pH = 4.75 (Scheme 1). The residual MO in the solution was analyzed by checking the absorbance at 464 nm with a UV−vis spectrophotometer (Varian Cary 100).

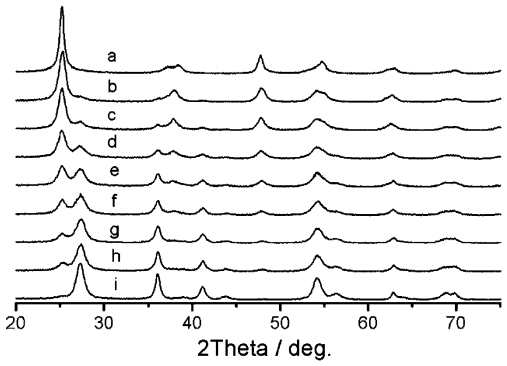

Figure 1. XRD patterns of TiO_2: (a) S-100, (b) S-1.60, (c) S-1.28, (d) S-1.12, (e) S-0.96, (f) S-0.80, (g) S-0.64, (h) S-0.32, and (i) S-0.00.

SCHEME 1: How MO Is Adsorbed on the TiO_2 Surface

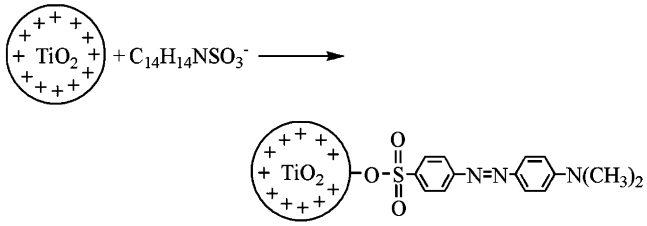

TABLE 1: Synthetic Conditions and Physicochemical Properties of TiO_2 Particles

sample	mole percent of SO_4^{2-} (%)	crystalline size of anatase[a] (nm)	crystalline size of rutile[a] (nm)	contents of anatase[b] (%)	S_{BET} (m^2/g)
S-0.00	0.00	14.5	9.4	0	88
S-0.32	0.32	15.9	11.1	9.8	162
S-0.64	0.64	15.0	11.2	15.3	169
S-0.80	0.80	12.0	11.6	36.0	147
S-0.96	0.96	13.0	10.5	52.4	131
S-1.12	1.12	12.5	12.1	74.2	113
S-1.28	1.28	12.9	15.9	89.3	86
S-1.60	1.60	17.7		100	
S-100	100			100	

[a] Calculated by eq 1. [b] Calculated by eq 2.

3. Results and discussion

3.1. Effect of the Proportion of Anion on Crystalline Phase Formation. The XRD patterns in Figure 1 illustrate the crystalline phases of different samples. As shown in Figure 1, the samples of S-100, S-1.60, and S-0.00 are pure anatase and rutile, respectively, while the other samples consist of both anatase and rutile. The contents of the anatase phases decrease in the order of S-1.60, S-1.28, S-1.12, S-0.96, S-0.80, S-0.64, S-0.32, and S-0.00. When the mole percentage of SO_4^{2-} is adjusted to more than 1.60% in the preparation procedure, only the anatase phase can be observed in the TiO_2 powder. That is to say, the content of the anatase phase increases with increasing concentration of SO_4^{2-} in the aqueous phase of the microemulsion in some range, and a large amount of SO_4^{2-} will only result in the presence of the anatase phase. The average crystalline sizes of anatase and rutile in the samples were calculated by applying the Debye−Scherrer formula[22] (eq 1) on the anatase (101) and rutile (110) diffraction peaks and are showed in Table 1.

$$D = \frac{K\lambda}{\beta \cos \theta} \tag{1}$$

where D is the average crystallite size in angstroms, K is a

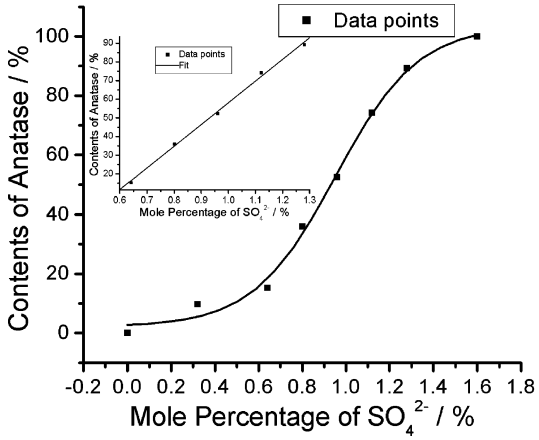

Figure 2. Relationship between the contents of anatase and the mole percentage of SO_4^{2-}. The inset shows the linear fit of samples S-1.28, S-1.12, S-0.96, S-0.80, and S-0.64.

constant which is taken as 0.89 here, λ is the wavelength of the X-ray radiation (Cu Kα = 0.154 06 nm), β is the corrected band broadening (full width at half-maximum (fwhm)) after subtraction of equipment broadening, and θ is the diffraction angle.

The phase contents of the samples can be estimated from the respective XRD peak intensities using the following equation[23]

$$f_A = \frac{1}{1 + \frac{1}{K}\frac{I_R}{I_A}} \qquad (2)$$

$$K = 0.79 \quad f_A > 0.2$$

$$K = 0.68 \quad f_A \le 0.2$$

where f_A is the fraction of anatase phase in the powder, and I_A and I_R are the X-ray intensities of the anatase (101) and rutile (110) diffraction peaks, respectively. The contents of the anatase phases in the samples were shown in Table 1. To study the relationship between the concentration of anion and the content of the anatase phase, we carried out a fit with these data and found that the relationship between the mole percentage of SO_4^{2-} in the Cl^- and SO_4^{2-} and the contents of anatase phase in TiO_2 powder presents an S-shaped curve (Figure 2). It is very interesting that the samples of S-1.28, S-1.12, S-0.96, S-0.80, and S-0.64 can be reasonably described by a linear relationship (Figure 2, inset). It implies that we could effectively control the contents of the anatase and rutile phases around the anatase contents of ~15−90% by simply varying the proportion of Cl^- and SO_4^{2-} in the aqueous phase of the microemulsion.

3.2. Analysis of UV−vis Diffuse Reflectance Spectra and FT-IR Spectra. UV−vis DRS of S-100, P25, S-1.12, S-0.80, and S-0.00 are presented in Figure 3. For the sample S-100 (pure anatase), the significant increase of the absorption at wavelengths shorter than 385 nm can be assigned to the intrinsic band-gap absorption of anatase. The band gap (E_g) is estimated to be 3.22 eV from the following equation[24]

$$\alpha(h\nu) = A(h\nu - E_g)^{m/2} \qquad (3)$$

where α is the absorption coefficient, $h\nu$ is the photon energy, and $m = 1$ for a direct transition between bands. This value is in accord with the reported value for anatase (3.2−3.3 eV).[25] The significant absorption of sample S-0.00 (pure rutile) started with 419 nm, exhibiting a band-gap value of 2.96 eV. For the

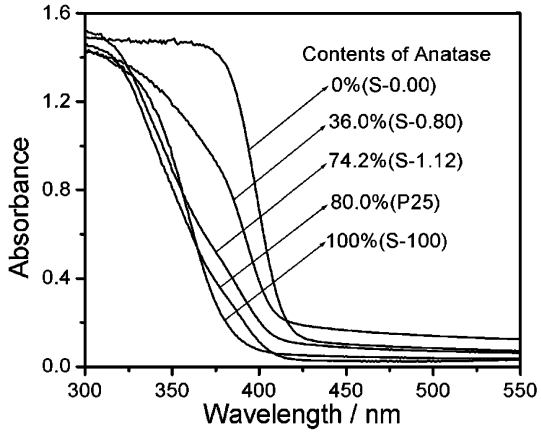

Figure 3. UV−vis diffuse reflectance spectra of S-100, P25, S-1.12, S-0.80, and S-0.00.

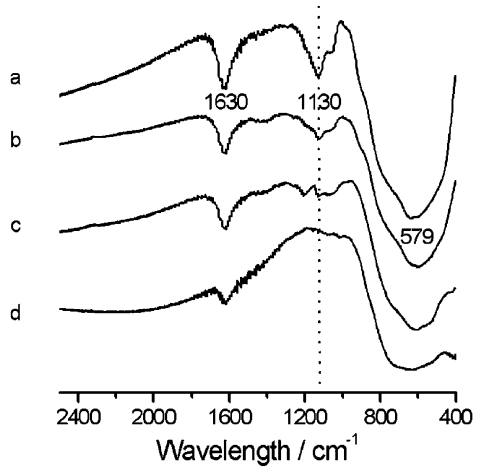

Figure 4. FT-IR spectra of (a) S-100, (b) S-1.28, (c) S-0.64, and (d) S-0.00.

other samples, the red shift of the absorption with respect to S-100 can be clearly observed in Figure 3 and increases in the order of P25, sample S-1.12, and S-0.80, whose band-gap values are 3.14, 3.11, and 3.00 eV, respectively. The order is very consistent with the increase of rutile content in the TiO_2 powder. The result implies that the difference of rutile content in the TiO_2 powder would influence the band-gap value of TiO_2.

To reveal the role of sulfate species in the preparation and crystallization of TiO_2, FT-IR spectra of the samples S-100, S-1.28, S-0.64, and S-0.00 were measured, as shown in Figure 4. Previous work[26,27] indicated that the surface-anchored SO_4^{2-} would present a characteristic FT-IR absorption band around 1250−1100 cm^{-1}. Thus, an intensity-changing IR signal around 1130 cm^{-1} should be the characteristic band of the bidentately bonding SO_4^{2-} species on the surface of TiO_2. The band at 1630 cm^{-1} corresponds to bending of the hydroxyl group adsorbed on the TiO_2 surface. Because anatase is more active than rutile in adsorbing the hydroxyl group, the increase of the rutile content in TiO_2 powder results in the decrease of the surface-adsorbed hydroxyl group.[28] The absorption intensity of the 1630 cm^{-1} band has a decreasing trend in the order of samples S-100, S-1.28, S-0.64, and S-0.00. The band at around 579 cm^{-1} is the stretching of the Ti−O group.[29] The absorption intensity at around 1130 cm^{-1} decreases in the order of samples S-100, S-1.28, and S-0.64. There is no absorption for sample S-0.00 at 1130 cm^{-1}, because it was prepared with hydrochloric acid. That is to say, an increase in the concentration of SO_4^{2-} in the preparation of TiO_2 led to an increase of bidentately bonding

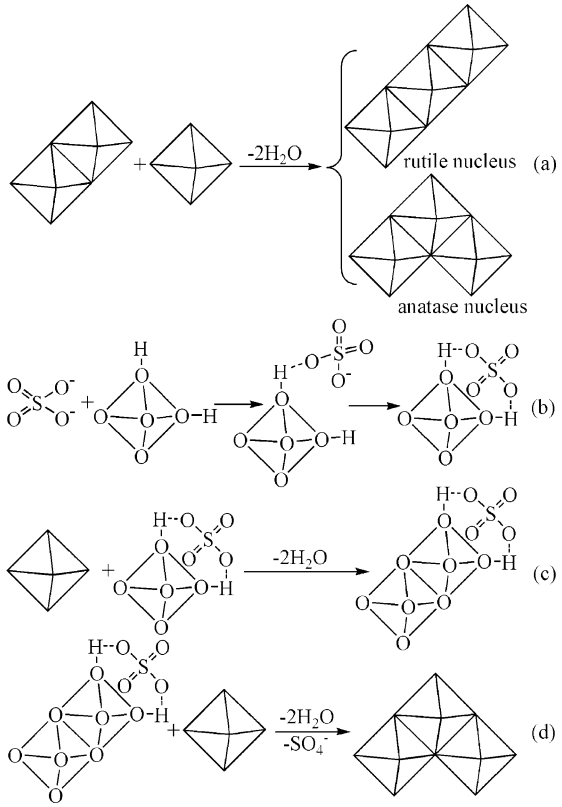

Figure 5. Proposed mechanism: (a) the orientation of the third octahedron determines whether a rutile or an anatase nucleus is formed; (b) interaction between SO_4^{2-} and TiO_6^{2-} octahedral hydroxyls; (c) two TiO_6^{2-} octahedra share edge in the presence of SO_4^{2-}; (d) formation of anatase in the presence of SO_4^{2-}.

SO_4^{2-} species on the surface TiO_2, and the surface bidentately bonding SO_4^{2-} would be involved in the crystalline phase formation process of TiO_2.

3.3. Mechanism of Forming Different Contents of Anatase. From metal alkoxide to the formation of metal oxide, there are two processes: hydrolysis and polycondensation.[30] When the titanic alkoxide reacts with water, the titanium ion first increases its coordination by using its vacant d orbitals to accept oxygen electron pairs from nucleophilic ligands (such as $-$OH groups).[31] Consequently, the titanium ion forms an octahedral structure of $Ti(O)_m(OH)_n(H_2O)_{6-m-n}^{(2m+n-4)-}$. Because the reaction is performed under an acidic medium, only $-$OH and $-OH_2$ groups will be present, and the octahedral structure of the titanium ion becomes $Ti(OH)_m(H_2O)_{6-m}^{(m-4)-}$.[32] Then, the structures dehydrate each other and polycondensed into the final precipitate. All TiO_2 crystal structures consist of TiO_6^{2-} octahedra, which share edges and corners in different manners that result in forming different crystal phases. Octahedra in anatase share four edges and are arranged in zigzag chains along [221], while rutile octahedra share only two edges and form linear chains parallel to [001].[32-35] The mechanism of forming anatase in the presence of SO_4^{2-} is proposed in Figure 5. For forming anatase and rutile nuclei, the placement of the third octahedron is very important and determines whether a rutile or an anatase nucleus is formed (Figure 5a).[32] However, the presence of SO_4^{2-} would influence the orientation of the third octahedron. When SO_4^{2-} ions exist in the acid reaction media, the SO_4^{2-} ion would interact with octahedral hydroxyls by static electricity (Figure 5b). It was confirmed from the SO_4^{2-} bidentately bonding to the titania in the FT-IR spectra (Figure 4). Similar observations have been reported previously in the case of SO_4^{2-} on ZrO_2 by the study of IR spectroscopy and theoretical calculations using an ab initio method.[36,37] Because of the steric effect of SO_4^{2-}, the octahedron with SO_4^{2-} and another octahedron would polycondense along the converse direction in order to decrease the repulsion (Figure 5c), and the orientation of the third octahedron is more conducive to the formation of an anatase nucleus (Figure 5d). The more SO_4^{2-} there are, the more anatase nuclei can be formed. The TiO_2 clusters grow further on the nucleus and then form the anatase phase. It has been reported that the presence of SO_4^{2-} accelerated the growth of TiO_2 clusters to anatase.[38] On the other hand, there is a weak steric effect for Cl^- because of its small radius. Meanwhile, the addition of Cl^- generally favors the formation of rutile crystallites.[39,40] As a result, different rutile/anatase mixtures can be prepared by changing the proportions of Cl^- and SO_4^{2-} in the aqueous phase of the microemulsion.

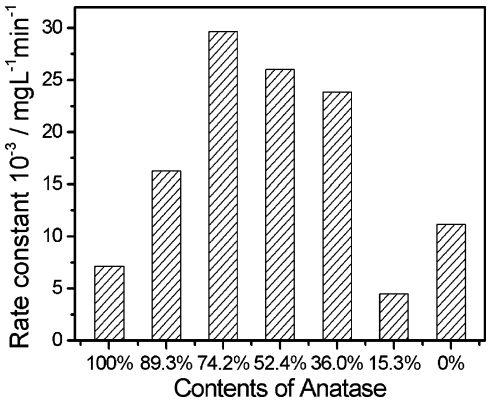

Figure 6. Rate constants for the photocatalytic decomposition of MO (40 mg L^{-1}) with different TiO_2 catalysts from left to right: S-100, S-1.28, S-1.12, S-0.96, S-0.80, S-0.64, and S-0.00.

3.4. Effect of the Proportion of Crystalline Phases on Photocatalytic Activity. Figure 6 shows the relationship between the apparent rate constants (mg L^{-1} min^{-1}) of MO (40 mg L^{-1}) degradation decolorization and the contents of anatase. The photocatalytic oxidation of MO is a pseudo-zero-order reaction and its kinetics may be expressed as follows: $C_0 - C = kt$, where k is the apparent reaction rate constant, and C_0 and C are the initial concentration and the reaction concentration of MO, respectively. In our experiments, all the solutions for photocatalytic reaction were in the weak acid condition, and the changes of pH were found to be very small. The possible reason may ascribe to the generation of amino-containing products from dimethyl amino- and azo- groups. In very low concentration, those amino-containing products might neutralize the generated hydrosulfate ions, and thus stabilize the pH value. From Figure 6, the photocatalytic activity of the samples increases with increasing anatase content at the beginning, and then has a downtrend with optimum photocatalytic activity at an anatase content of 74.2%. Sample S-0.64 containing 15.3% anatase has the worst photocatalytic activity for the photodegradation of MO. One possible reason may be its large surface area with relatively inferior crystallite (see Figure 1). It has been reported that electron$-$hole recombination on the particle surface would be enhanced by an increase in surface defects with increasing surface area.[41] The BET surface areas of all samples are shown in Table 1. The S_{BET} values of S-100 (pure anatase) and S-0.00 (pure rutile) are very similar, and both of them are far less than those of the other samples. For the other samples, there is a downtrend of the S_{BET} with an increase of the anatase content. The S_{BET} of sample S-1.12 with the highest photocatalytic activity is only 131 m^2/g, while the BET surface area of sample S-0.64 with the worst photocatalytic activity achieves 162 m^2/g. This result implies that surface area

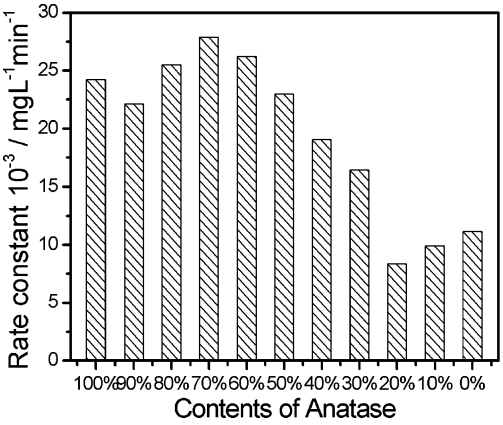

Figure 7. Rate constants for the photocatalytic decomposition of MO (40 mg L^{-1}) with physically mixed TiO_2 catalysts.

is not a main factor for photocatalytic activity in our experiments. On the other hand, it was reported that the presence of SO_4^{2-} would inhibit the degradation of a simulated contaminant, because the SO_4^{2-} ions compete with the contaminant for adsorption on the TiO_2 surface.[42] However, the adsorption of MO was not obviously changed with the different samples in our experiments, and the photocatalytic activities of the mixed-phase samples are not in accord with the adsorbance of SO_4^{2-}. Therefore, the difference of the anatase content and the photoelectrochemical interaction between the anatase and rutile phases should be the main factors that decide the photocatalytic activity in the mixed-phase samples. That is to say, anatase and rutile have a synergistic effect in enhancing the photocatalytic activity of TiO_2. To further confirm the synergistic effect of anatase and rutile, different anatase/rutile ratios in TiO_2 catalysts were achieved by physically mixing pure anatase and pure rutile. Figure 7 shows the apparent rate constants (mg L^{-1} min^{-1}) of MO (40 mg L^{-1}) for degradation with physically mixed TiO_2 as catalysts. As shown in Figure 7, there is a similar result to Figure 6 in the relationship between the photocatalytic activity and the content of anatase. The sample containing about 70% anatase showed the highest photocatalytic activity for photodegradation of MO, while the sample containing about 20% anatase showed the worst photocatalytic activity.

$$TiO_2 \xrightarrow{h\nu} e_{CB}^- + h_{VB}^+ \quad (4)$$

$$e_{CB}^- \rightarrow e_{tr}^- \quad (5)$$

$$h_{VB}^+ \rightarrow h_{tr}^+ \quad (6)$$

In the photocatalytic reaction mechanism of TiO_2, the primary step is the photogeneration of pairs of electrons and holes in the TiO_2 particles (eq 4). Trapping of the electrons within less than 500 fs[43] (eq 5) and holes within less than 30 ps[44] (eq 6) occur. Then, the photooxidations are initiated by surface-trapped holes (h_{tr}^+) and not by valence band holes (h_{VB}^+).[44,45] Because anatase and rutile differ mainly in the position of the conduction band edge, for which that of anatase is above that of rutile.[46] When anatase interweaves with rutile, the electrons in the anatase phase would transfer into rutile, while the holes transfer from rutile to anatase. Therefore, the anatase/rutile mixed phase could hinder electron−hole recombination by locating the electron and the hole in different crystalline phases. On the other hand, the rutile phase with a narrower band gap could extend the useful range of the photoresponse and harvest more light. Therefore, the mixed phase promotes efficiency of the photons of TiO_2. As a result, the anatase/rutile mixed phase shows a synergistic effect in enhancing the photocatalytic activity. When the content of rutile is too little, it may be surrounded with too many anatase particles,[12] and the charge transfer between rutile and anatase is limited to some extent. On the other hand, a low content of rutile cannot extend the photoresponsive range so effectively. However, in the presence of too much rutile, rutile would absorb much light, which inhibits the photoexcition happening in the anatase phase. Therefore, the photocatalytic activity of TiO_2 is also lower, because rutile is not as good a photocatalytic phase as anatase, in the general opinion. As a result, the optimum proportion of anatase and rutile was found to be about 3:1 in our experiments.

4. Conclusions

Nanocrystalline TiO_2 catalysts of high surface area and different anatase/rutile ratios have been prepared by the MMH method at low temperature. By simply varying the proportion of Cl^- and SO_4^{2-} in the aqueous phase of the microemulsion, the different contents of anatase and rutile phases in the powders have been successfully controlled precisely. Different red shifts of the UV−vis absorption of the samples are observed because of the different contents of the rutile phase in samples. It was found that bidentately bonding SO_4^{2-} species on TiO_6^{2-} octahedra is a main factor that affects the crystallite phase formation of TiO_2 during the preparation process. The catalyst containing 74.2% anatase showed the highest photocatalytic activity for photodegradation of MO, which is due to a synergistic effect between anatase and rutile. The synergism was also found for the photodegradation of MO with physically mixed TiO_2 with different anatase/rutile ratios as catalysts.

Acknowledgment. This work has been supported by the Program for New Century Excellent Talents in University, the National Nature Science Foundation of China (20407007), the Shanghai Nanotechnology Promotion Center (0452nm010), and the National Basic Research Program of China (2004CB719500).

References and Notes

(1) Fujishima, A.; Honda, K. *Nature (London)* **1972**, *238*, 37.
(2) Zhu, J.; Zheng, W.; He, B.; Zhang, J.; Anpo, M. *J. Mol. Catal. A* **2004**, *216*, 35.
(3) Zhang, J.; Ayusawa, T.; Minagawa, M.; Kinugawa, K.; Yamashita, H.; Matsuoka, M.; Anpo, M. *J. Catal.* **2001**, *198*, 1.
(4) Zhang, J.; Hu, Y.; Matsuoka, M.; Yamashita, H.; Minagawa, M.; Hidaka, H.; Anpo, M. *J. Phys. Chem. B* **2001**, *105*, 8395.
(5) Park, D. R.; Zhang, J.; Ikeue, K.; Yamashita, H.; Anpo, M. *J. Catal.* **1999**, *185*, 114.
(6) Okamoto, K.; Yamamoto, Y.; Tanaka, H.; Tanaka, M.; Itaya, A. *Bull. Chem. Soc. Jpn.* **1985**, *58*, 2015.
(7) Zhang, Q.; Gao, L.; Guo, J. *Appl. Catal., B* **2000**, *26*, 207.
(8) Sclanfani, A.; Palmosano, L.; Schiavello, M. *J. Phys. Chem.* **1990**, *94*, 829.
(9) Yu, J. C.; Yu, J.; Ho, W.; Zhang, L. *Chem. Commun.* **2001**, 1942.
(10) Bacsa, R. R.; Kiwi, J. *Appl. Catal., B* **1998**, *16*, 19.
(11) Yu, J. C.; Lin, J.; Kwok, R. W. *J. Photochem. Photobiol. A* **1997**, *111*, 199.
(12) Ohno, T.; Tokieda, K.; Higashida, S.; Matsumura, M. *Appl. Catal., A* **2003**, *244*, 383.
(13) Bickley, R. I.; Gonzalez-Carreno, T.; Lees, J. S.; Palmisano, L.; Tilley, J. D. *J. Solid State Chem.* **1991**, *92*, 178.
(14) Datye, A. K.; Riegel, G.; Bolton, J. R.; Huang, M.; Prairie, M. R. *J. Solid State Chem.* **1995**, *115*, 236.
(15) Ohno, T.; Sarukawa, K.; Tokieda, K.; Matsumura, M. *J. Catal.* **2001**, *203*, 82.
(16) Hurum, D. C.; Agrios, A. G.; Gray, K. A.; Rajh, T.; Thunauer, M. C. *J. Phys. Chem. B* **2003**, *107*, 4545.
(17) Yang, J.; Huang, Y. X.; Ferreira, J. M. *J. Mater. Sci. Lett.* **1997**, *16*, 1933.
(18) Yang, J.; Ferreira, J. M. *Mater. Res. Bull.* **1998**, *33*, 389.
(19) Luo, H.; Wang, C.; Yan, Y. *Chem. Mater.* **2003**, *15*, 3841.

(20) Liu, W.; Chen, A.; Lin, J.; Dai, Z.; Qiu, W.; Liu, W.; Zhu, M.; Usuday, S. *Chem. Lett.* **2004**, *33*, 390.
(21) Wu, M.; Long, J.; Huang, A.; Luo, Y. *Langmuir* **1999**, *15*, 8822.
(22) Lin, J.; Lin, Y.; Liu, P.; Meziani, M. J.; Allard, L. F.; Sun, Y. *J. Am. Chem. Soc.* **2002**, *124*, 11514.
(23) Spurr, R. A.; Myers, H. *Anal. Chem.* **1957**, *29*, 760.
(24) Sanchez, E.; Lopez, T. *Mater. Lett.* **1995**, *25*, 271.
(25) Linsebigler, A. L.; Lu, G.; Yates, J. T., Jr. *Chem. Rev.* **1995**, *95*, 735.
(26) Samantaray, S. K.; Mishra, T.; Parida, K. M. *J. Mol. Catal. A* **2000**, *156*, 267.
(27) Samantaray, S. K.; Mohapatra, P.; Parida, K. *J. Mol. Catal. A* **2003**, *198*, 277.
(28) Ding, Z.; Lu, G. Q.; Greenfield, P. F. *J. Phys. Chem. B* **2000**, *104*, 4815.
(29) Tanaka, Y.; Suganuma, M. *J. Sol−Gel Sci. Technol.* **2001**, *22*, 83.
(30) Wang, C.; Ying, J. Y. *Chem. Mater.* **1999**, *11*, 3113.
(31) Livage, J.; Henry, M.; Sanchez, C. *Prog. Solid State Chem.* **1988**, *18*, 259.
(32) Gopal, M.; Chan, W. J. M.; De Jonghe, L. C. *J. Mater. Sci.* **1997**, *32*, 6001.
(33) Fahmi, A.; Minot, C.; Fourre, P.; Nortier, P. *Surf. Sci.* **1995**, *343*, 261.
(34) Penn, R. L.; Banfield, J. F. *Am. Mineral.* **1999**, *84*, 871.
(35) Li, Y.; White, T. J.; Lim, S. H. *J. Solid State Chem.* **2004**, *177*, 1372.
(36) Babou, F.; Bigot, B.; Sautet, P. *J. Phys. Chem.* **1993**, *97*, 11501.
(37) Babou, F.; Coudurier, G.; Vedrine, J. C. *J. Catal.* **1995**, *152*, 341.
(38) Zhang, Q.; Gao, L.; Guo, J. *J. Eur. Ceram. Soc.* **2000**, *20*, 2153.
(39) Zhang, Q.; Gao, L. *Langmuir* **2003**, *19*, 967.
(40) Kittaka1, S.; Matsuno, K.; Takahara, S. *J. Solid State Chem.* **1997**, *132*, 447.
(41) Ohtani, B.; Iwai, K.; Kominami, H.; Matsuura, T.; Kera, Y.; Nishimoto, S. *Chem. Phys. Lett.* **1995**, *242*, 315.
(42) Yamazaki, S.; Fujinaga, N.; Araki, K. *Appl. Catal., A* **2001**, *210*, 97.
(43) Colombo, D. P., Jr.; Roussel, K. A.; Saeh, J.; Skinner, D. E.; Cavaleri, J. J.; Bowman, R. M. *Chem. Phys. Lett.* **1995**, *232*, 207.
(44) Serpone, N.; Lawless, D.; Khairutdinov, R.; Pelizzetti, E. *J. Phys. Chem.* **1995**, *99*, 16655.
(45) Lawless, D.; Serpone, N.; Meisel, D. *J. Phys. Chem.* **1991**, *95*, 5166.
(46) Kavan, L.; Gratzel, M.; Gilbert, S. E.; Klemenz, C.; Scheel, H. J. *J. Am. Chem. Soc.* **1996**, *118*, 6716.